Proceedings of the ASME 2011 5th International Conference on Energy Sustainability
ES2011
August 7-10, 2011, Washington, DC, USA

ES2011-54173

NUMERICAL ANALYSIS OF A ROOFTOP VERTICAL AXIS WIND TURBINE

Uzarraga-Rodriguez N. Cristobal, Gallegos-Muñoz A. and Riesco Ávila J. Manuel

Department of Mechanical Engineering
University of Guanajuato
Salamanca, Guanajuato, Mexico

ABSTRACT

A numerical analysis of a rooftop vertical axis wind turbine (VAWT) for applications in urban area is presented. The numerical simulations were developed to study the flow field through the turbine rotor to analyze the aerodynamic performance characteristics of the device. Three different blade numbers of wind turbine are studied, 2, 3 and 4, respectively. Each one of the models was built in a 3D computational model. The effects generated in the performance of turbines by the numbers of blades are considered. A Sliding Mesh Model (SMM) capability was used to present the dimensionless form of coefficient power and coefficient moment of the wind turbine as a function of the wind velocity and the rotor rotational speed. The numerical study was developed in CFD using FLUENT®. The results show the aerodynamic performance for each configuration of wind turbine rotor. In the cases of Rooftop rotor the power coefficient increases as the blade number increases, while in the case of Savonius rotor the power coefficient decrease as the blades number increases.

Keywords: Wind energy, rooftop turbine, vertical axis wind turbine, torque coefficient and power coefficient.

1. INTRODUCTION

In the last years, the renewable energy sources have acquired a great interest in the area of electric power generating. Due to growing concern to reduce the effects of climate change, such as global warming, generated by extensive and deliberate use of fossil fuels, mainly in the electric power generating and transport. The wind power is one of the renewable energy sources most attractive to meet the production and demand of electric energy on commercial and industrial applications, since it is a clean, economic and renewable energy source with a great availability in the environment.

The wind turbines are devices used for electric energy generation from wind kinetic energy. These turbines can be classified into two main classes, which are horizontal and vertical axis. Currently, the most wind power systems consist in the uses of horizontal axis wind turbine (HAWT). These turbine require complicated structure that are difficult to install and maintenance, are economically valuable only in areas where the permanent winds and high speeds are available. The HAWT provide a greater efficiency due to the high rotation speed. However, they are not necessary for all purposes.

On the other hand, in an urban environment the speed and direction wind are always changing. In these conditions, the vertical axis wind turbines (VAWT) can be used more effectively within the urban areas to increase the electrical power generation capacity to small-scale. Unlike horizontal axis turbine, the vertical axis turbines are made up of simple structure, the rotation speed is low and torque is high. Also, these turbines are independent of the wind direction [1].

The numerical and experimental study of aerodynamic behavior of the vertical axis wind turbines has been a topic widely studied in literature, both static and dynamic conditions of the wind turbine rotor. Ushiyama I. *et al.* [2], Sheldahl RE. *et al.* [3], Alexander AJ. *et al.* [4], Modi VJ. *et al.* [5] y Mojola OO. *et al.* [6 and 7] have developed studies about this topic experimental and numerically. These studies are mainly focused on the aerodynamics effects generated by different

implementation and modifications to the geometric parameters of the Savonius rotor, such as the variation of rotor aspect ratio, the number of blade, the separation gap and the overlap between rotor blade and the profile change of the blade cross-section. However, there is little information on other rotor geometry of the vertical axis wind turbine.

On the other hand, the computational advances have allowed developing important numerical studies, analyzing the flow around the wind turbine rotor. Altan D.A. *et al.* [8 and 9] developed a numerical and experimental analysis of the effect caused by curtain systems on the low performance levels of the Savonius wind rotor in static conditions. Results show to increase the performance of the Savonius wind rotor, a curtain arrangement as a simple wind deflector has been designed and placed in front of the rotor with aim of preventing the negative torque. Having that the best performance has been obtained from curtain 1 at its position θ = 60º for the angles β = 15º and α = 45º. K. Pope *et al.* [10] developed numerical and experimental studies to determine the operating performance and power output from a Zephyr vertical axis wind turbine. The 3-D numerical predictions were based on the time averaged Spalart-Allmaras equations. Results show that the prediction of power coefficient (C_P) obtained with the sliding mesh formulation was 0.111, having a 13.3% difference compared to the Multiple Reference Frame (MRF) prediction.

Recently, D'Alessandro V. *et al.* [11] developed a numerical and experimental analysis of the aerodynamic behavior of Savonius wind rotor in dynamic conditions. In the numerical analyses was used a SMM (Sliding Mesh Model) approach available in the CFD code FLUENT. A mathematical model of the interaction between the flow field and the rotor blades was developed and validated by comparing its results with data obtained experimentally.

The present study shows a numerical analysis focused to predict the aerodynamic behavior of a rooftop vertical axis wind turbine by mean the uses Sliding Mesh Model (SMM) approach. The result shows the power coefficient of rooftop and Savonius wind rotor. The numbers of blades are varied. The results are compared with data obtained from Savonius wind rotor.

2. NUMERICAL ANALYSIS

The generation of the model mesh, governing equation, assignation of the boundary conditions and solution formulations will be discussed in this section. In order to develop the CFD simulations the commercial software FLUENT 6.3.26 [12] was used. The considerations used in this study were: transient state, Newtonian fluid, rotating frame adaptation of the governing equation, RNG *k*-ε model.

2.1 Governing Equations

Since the cross-flow turbine rather slowly, the flow is governed by incompressible form of the Reynolds averaged Navier-Stokes (RANS). The governing equations for the flow fluid include the following equations

Mass conservation

$$\frac{\partial \rho}{\partial t} + \frac{\partial}{\partial x_i}\left(\rho \overline{u_\iota} + \rho \overline{u'_\iota}\right) = 0 \tag{1}$$

Momentum

$$\frac{\partial}{\partial t}(\rho \overline{u_\iota}) + \frac{\partial}{\partial x_i}\left(\rho \overline{u_\iota u_j}\right) + \rho(2\vec{\omega} \times \overline{u_\iota} + \vec{\omega} \times \vec{\omega} \times \vec{r}) = -\frac{\partial \bar{p}}{\partial x_j} + \frac{\partial \left(\overline{\tau_{\iota J}}\right)_{eff}}{\partial x_i} \tag{2}$$

The momentum equation contains two additional terms, which are the Coriolis acceleration and the centripetal acceleration respectively. In this equation, $\vec{\omega}$ is the angular velocity of the rotor domain and $\vec{r}$ is the radial position from the origin of the rotating domain [12].
The viscous stress $\left(\overline{\tau_{ij}}\right)_{\text{eff}}$ given by equation (2), is calculated as following:

$$\left(\overline{\tau_{\iota J}}\right)_{eff} = \mu_{eff}\left(\frac{\partial \overline{u_\iota}}{\partial x_j} + \frac{\partial \overline{u_j}}{\partial x_i} - \frac{2}{3}\delta_{ij}\frac{\partial \overline{u_k}}{\partial x_k}\right) - \rho \overline{u'_\iota u'_j} \tag{3}$$

The transport equations considerate for the turbulences quantities from RNG *k*-ε model are described by Equations (4) and (5).

$$\frac{\partial}{\partial t}(\rho k) + \frac{\partial}{\partial x_i}(\rho k u_i) = \frac{\partial}{\partial x_j}\left(\alpha_k \mu_{eff}\frac{\partial k}{\partial x_j}\right) + G_k - \rho\varepsilon \tag{4}$$

$$\frac{\partial}{\partial t}(\rho \varepsilon) + \frac{\partial}{\partial x_i}(\rho \varepsilon u_i) = \frac{\partial}{\partial x_j}\left(\alpha_\varepsilon \mu_{eff}\frac{\partial \varepsilon}{\partial x_j}\right) + C_{1\varepsilon}\frac{\varepsilon}{k}G_k - C_{2\varepsilon}\rho\frac{\varepsilon^2}{k} - R_\varepsilon \tag{5}$$

In these equations, G_k represents the generation of turbulent kinetic energy due to the mean velocity gradients, the quantities α_k and α_ε are the inverse effective Prandtl numbers for *k* and ε, respectively. The effective Viscosity, μ_{eff}, is calculated by the combination of the turbulent kinetic energy (*k*) and the dissipation ratio (ε),

2.2 Geometry

Figure 1 shows the rotor geometry of the Rooftop and Savonius vertical axis wind turbine. In this figure can be seen the Rooftop and Savonius rotors with two bladed, three bladed and four bladed, which were analyzed in this study.

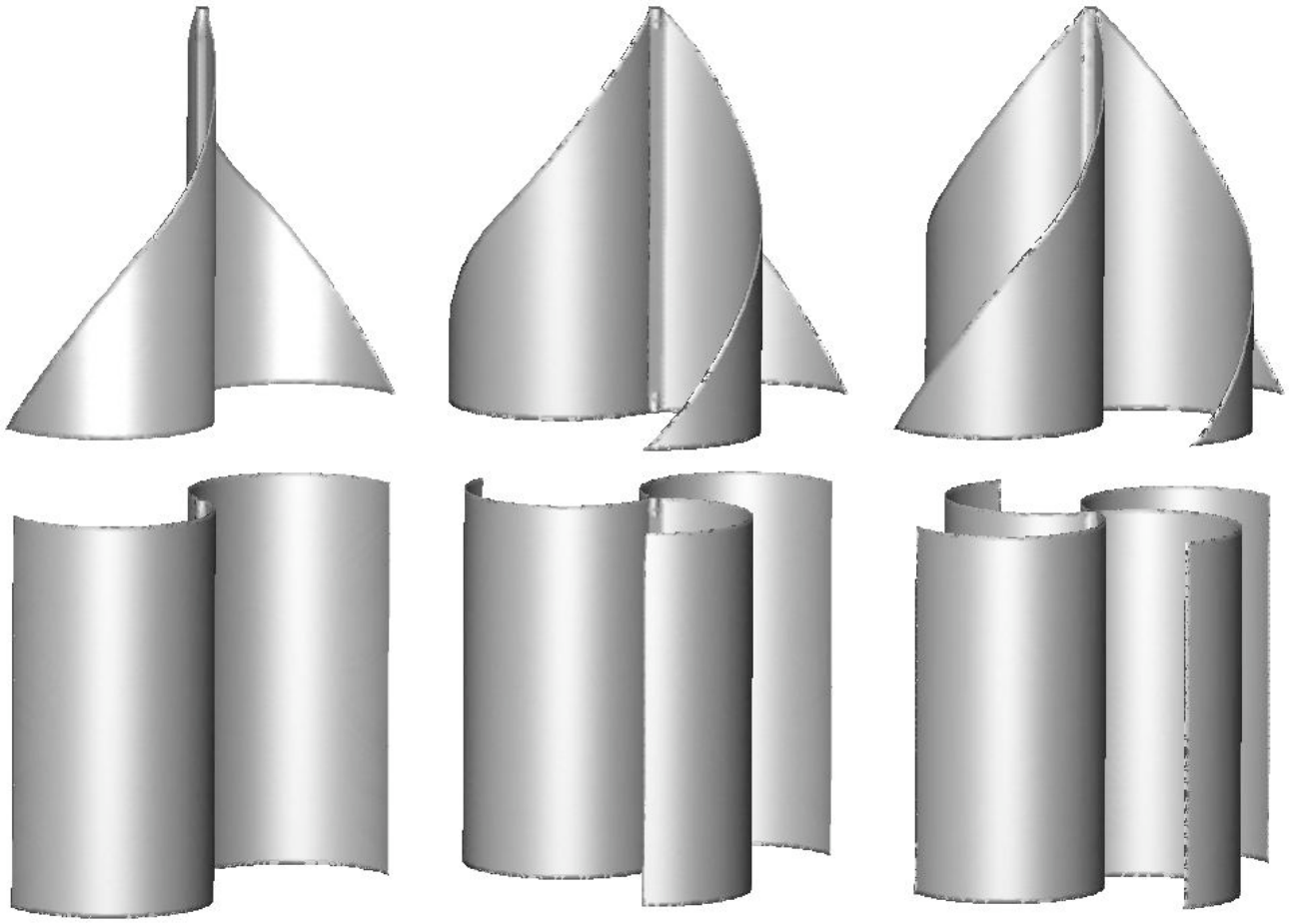

a) *b)* *c)*

Figure 1. *Rooftop and Savonius rotors geometry with a) two bladed , b) three bladed and c) four bladed, respectively.*

In the Figure 2 can be seen a sketch of the geometrical variables of wind rotors.

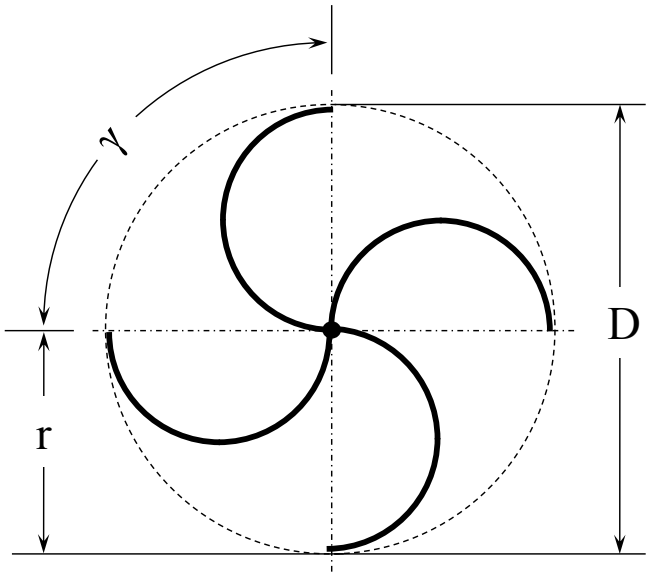

Figure 2. *Sketch of the geometrical variables of wind rotor.*

In the Table 1 are present the geometrical variables of the two bladed, three bladed and four bladed wind rotors.

Table 1. *Geometric variables of the wind rotors.*

No. Blade	D (m)	γ (deg)	H (m)
Two	0.32	180	0.3
Three	0.32	120	0.3
Four	0.32	90	0.3

where D is the rotor diameter and H is the rotor height.

2.3 Computational grid

Numerical simulations have been development using computational mesh generating in the preprocessor GAMBIT [13]. All grids were structured by mixed cells (hexahedral and prismatic elements). These grids are not uniform in all directions. For the grid used in the computational models, the mesh density is high in the near zone to the walls of the wind rotors. The Figure 3 shows the grid used in this study. This configuration of mesh was used for all wind rotors.

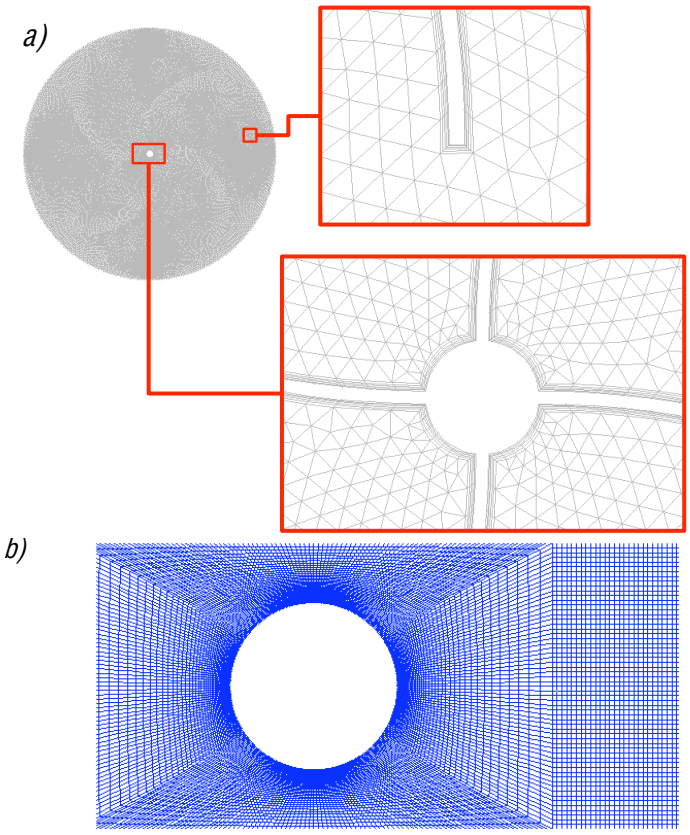

Figure 3. *Computational grid of the VAWT. a) Rotating sub-domain that include the rotor and b) stationary sub-domain or surrounding.*

In order to solve a 3D unsteady flow, sliding mesh model (SMM) was used. In this technique, the overall computational domain is divided into two sub-domains. For the wind rotor, a circular sub-domain containing the turbine blade rotates at the turbine rotational speed, while the remaining sub-domain exterior to the turbine blade is stationary. During the calculation, the turbine blade sub-domain slides relative to stationary sub-domain along the grid interface in discrete steps, and the unsteady Reynolds Average Navier-Stokes equations are solved in the moving coordinate system. At the sliding mesh interface between the rotating sub-domain and the stationary sub-domain, flow variables and their gradients are carefully interpolated so that mass conservation and accuracy of the numerical scheme are preserved [14].

The computational grids have a total of 1492912 mixed cells for a three-dimensional simulation, which 40% of this total corresponding to rotating sub-domain and 60% to the stationary sub-domain. In the Figures 3b can be seen that the stationary sub-domain presents a high quantity of hexahedral elements.

2.4 Boundary conditions and physical proprieties of fluid

The governing equations require the specification of boundary conditions at the inlet, outlet and wall due to elliptic nature of the equations. The boundary conditions applied in the computational model of VAWTs are presented in Figure 4.

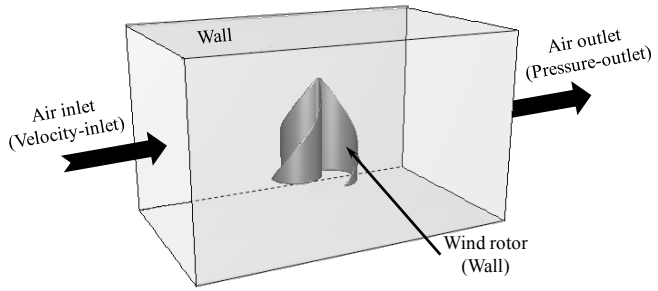

Figure 4. *Boundary conditions in the computational model of the vertical axis wind turbines.*

In the Table 2 and Table 3 are summarized the boundary condition and physical proprieties of fluid, respectively.

Table 2. Boundary conditions.

Air flow inlet	
Velocity-inlet	5-8 [m/s]
Turbulent intensity (T_i)	10 % [-]
Hydraulic diameter (D_h)	0.6 [m]
Air flow outlet	
Static pressure outlet	101325 [Pa]
Backflow turbulent intensity (T_i)	12 % [-]
Backflow hydraulic diameter (D_h)	0.6 [m]
Walls tunnel	
Stationary (*Motion condition*)	
No slip (*Shear condition*)	
Walls rotor	
Moving relative to adjacent cell zone (*Motion condition*)	
No slip (*Shear condition*)	

Table 3. Physical proprieties of air flow.

Density	1.225 [kg/m^3]
Viscosity	1.7894 e^{-05} [kg/m·s]

As mentioned above, one of the boundary conditions required in the sliding mesh model is an interface between rotating and stationary sub-domains in order to allow the transient prediction of the rotor interaction with the flow field. The Figure 5 presents the overall computational domain where the interface between rotating and stationary sub-domain is showed.

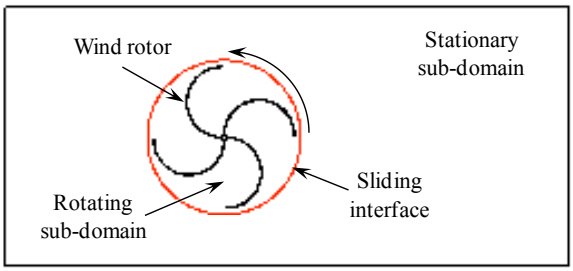

Figure 5. *Overall computational domain of the VAWTs.*

2.5 Rotor performance parameter

Rotors of different sizes can be compared by performance parameter [15]. The performance parameters commonly used in the aerodynamics of wind turbine are normally expressed in dimensionless form. These performance parameters are the moment coefficient and the power coefficient, which are calculated as following:

$$C_m = \frac{M}{\frac{1}{2}\rho U_\infty^2 Ar} \tag{6}$$

$$C_P = \frac{P}{\frac{1}{2}\rho U_\infty^3 A} \tag{7}$$

where $A = D \bullet H$ is the frontal rotor area. The performance parameters were evaluated as function of the dimensionless parameter tip-speed ratio, which is calculated as following:

$$\lambda = \frac{\omega D}{2U_\infty} \tag{8}$$

The equations (6) and (7) can be related by the following equation:

$$C_m = \frac{C_P}{\lambda} \tag{9}$$

2.6 Computational method

The aerodynamic performance of a Rooftop and Savonius wind axis vertical turbines with different blade number was realized using the commercial code FLUENT® version 6.3.26 [12]. This code allows to solve the Reynolds averaged Navier-Stokes and the transport equations of the turbulences quantities. The RNG k-ε turbulence model was derived from the instantaneous Navier-Stokes equations, using a mathematical technique called renormalization group [16]. This model has an additional term in dissipation ration (ε) equation that significantly improves the accuracy for rapidly strained flows. Also, the effect of swirl on turbulence is included, enhancing accuracy for swirling flow. The SIMPLE algorithm was used to link the velocity field and pressure distribution inside the computational models. This algorithm uses a relation between the velocity and pressure in order to satisfy the mass conservation, getting a velocity field. In the unsteady sliding mesh calculation, the time step taken was 1/160th of the wind rotor period, that is to say, 160 time step per revolution.

All numerical simulations were realized applying the pressure-based solver, with this approach the governing equations (continuity and momentum) are solved simultaneously. Due to the governing equations are no-linear and coupled, several iterations were developed to reach the solution convergence per each time step. The algebraic linear equations system defined in FLUENT were solved with the Gauss-Seidel linear algorithm. The convergence criterion used in the iterative numerical scheme is established according to the computational software. Thus the Reynolds averaged Navier-Stokes and the turbulence quantities equations reach the convergence when the residual has value of 10^{-5}, while the conservation mass equation reaches the convergence with 10^{-6} residual. Two computers were used to solve the models. Each computer is formed a processor i7 with 3.6 GHz and 12 GB in RAM. These equipments are connected in a parallel processing.

3. RESULTS AND DISCUSSIONS

The results show a comparison between numerical data of moment coefficient (C_m) as function of the angular position, to Rooftop and Savonius rotors. Also, it is presented the behavior of power curve and moment curve for the Rooftop and Savonius rotors, evaluated as function of the dimensionless parameter Tip-speed ratio (λ). The results are obtained for different numbers of blades. Finally, is showed the comparison of the maximum power curve obtained from Rooftop and Savonius rotors.

3.1 Comparison with experimental data

A qualitative comparison between the pressure distribution obtained numerically in this study and the pressure distribution obtained experimentally by Fernando M.S.U.K [17] was carried out to compare the external flow around the blade rotors. The basic blade shape and optimum blade parameters used by [17] are show in the Figure 6 and Table 4, respectively.

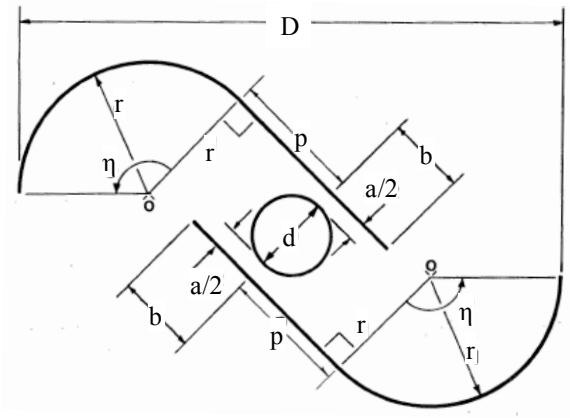

Figure 6. *Basic blade shape and the associated parameters.*

Table 4. Optimum blade parameters.

Parameter	Description	Value
a/D	non-dimensional blade gap-size	0
b/D	non-dimensional overlap	0
p/r	Blade shape parameter	0.2
η	blade arc angle	135 º

They measured the pressure distribution on the two bladed Savonius rotor. The pressure measurements were made at 46 pressures tapping on the blade rotor. The pressure was measured at 10º intervals form 0º to 360º. The numerical and experimental data of static pressure were normalized by mean of pressure coefficient given by equation (10), which is calculated as following:

$$C_p = \frac{(p_i - p_\infty)}{\frac{1}{2}\rho U_\infty^2} \qquad (10)$$

where p_i is the static pressure measured at the i[th] point and p_∞ is the static pressure at infinity.

The Figure 7 shows the comparison between the numerical and experimental pressure distribution at the midspan of the blade rotor at flow angle 30º. In the front side of blade rotor, the numerical results show to agree with experimental results for a distance along surface from 0 to 0.72. In this section, the average difference is 3% respect to experimental data, at range of variation of 0.7 to 35%. Then numerical and experimental results show difference.

On other hand, it can be seen that the pressure distribution, corresponding to numerical data on the back side of the blade rotor, it is agrees with the experimental data, having an average difference of 2.5% at range of variation of 2 to 45%.

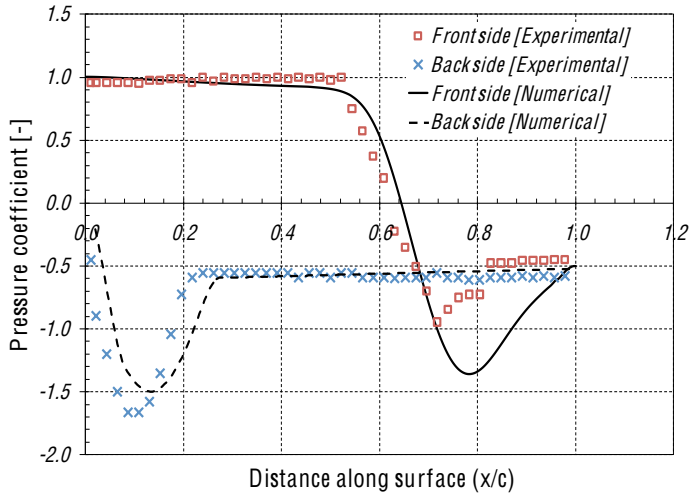

Figure 7. *Comparison of pressure distribution around the blade rotor.*

3.2 Moment coefficient as function of angular position

Figures 8 and 9 showed the moment coefficient for two bladed, three bladed and four bladed rotors as function of the angular position for both rotors. In the case of two bladed Rooftop rotor, the moment coefficient decrease from θ = 0º rotor angle reaching its minimum value at θ = 90º, which become negative. It then increases up to θ = 170º reached its maximum value. Then the behavior becomes periodic, having a period each 180º rotor angle. For the case of three bladed Rooftop rotor, the maximum value of moment coefficient is reached at θ = 10º reaching its maximum. Its minimum value occurs at θ = 55º. This periodic behavior has a period each 120º rotor angle. In the case of four bladed Rooftop rotor, the moment coefficient increase from θ = 0º to θ = 25º reaching its maximum value. It then decrease up to θ = 60º reached its minimum value. Then the periodic behavior has a period each 90º rotor angle.

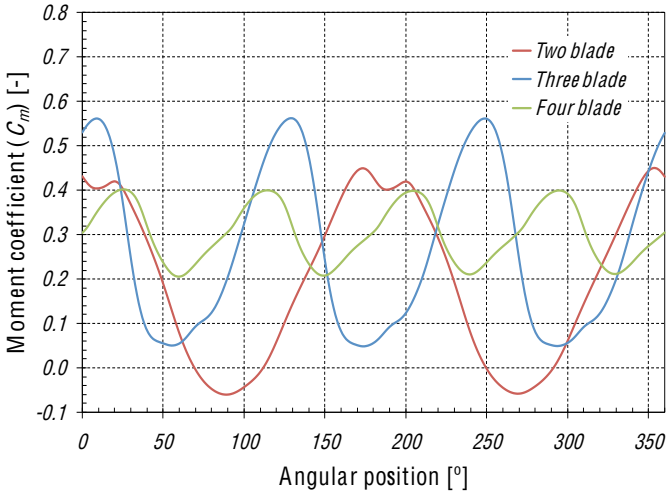

Figure 8. *Variation of moment coefficient (C_m) for two bladed, three bladed and four bladed Rooftop rotors.*

In the case of two bladed Savonius rotor, the moment coefficient increase rapidly from θ = 0º to θ = 40º reaching its maximum value. It then decrease suddenly up θ = 80º, then continues decrease smoothly from θ = 80º to θ = 110º reached the minimum value, which become negative. Then the periodic behavior has a period each 180º rotor angle. In the cases of three bladed and four bladed rotors present the same behavior, with increment and decrement smoother, as compared with the two blades Savonius rotor. For three bladed Savonius rotor the maximum values is reached at θ = 35º, while that the four bladed Savonius rotor reach its maximum value at θ = 40º. The minimum values for three bladed and four bladed Savonius rotors occurs at θ = 80º and θ = 70º, respectively. The three bladed Savonius rotor has a period each θ = 120º, while that the four bladed Savonius rotor has a period each θ = 90º rotor angle.

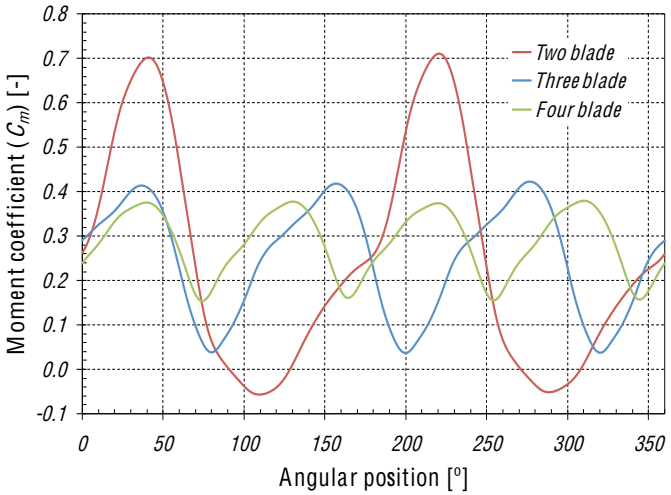

Figure 9. *Variation of moment coefficient (C_m) for two bladed, three bladed and four bladed Savonius rotors.*

Also can be seen in the Figure 8 and 9 that the period per turbine rotor revolution increase as the numbers of blade increase, while that amplitude decrease as the number of blade increases. This behavior is similar in both rotors. Comparing the results show in the Figures 8 and 9, it is possible observe that Rooftop rotors produce an initial moment coefficient large that Savonius rotors at $\theta = 0^{o}$ rotor angle. This effect on the behavior of the moment coefficient may be due to the triangular geometry of Rooftop rotor. Allows the vortices are generated between the blades of Rooftop rotor. This allows increase the efficiency of energy extraction, due to addition of lift force to drag force that acts on the blade rotor.

3.3 Moment coefficient as function of tip-speed ratio

Figures 10 and 11 showed the moment coefficient for two bladed, three bladed and four bladed rotors as function of the dimensionless parameter tip-speed ratio. In the Figure 10 are showed the results obtained from Rooftop rotors. In general, the moment coefficient decrease nearly linear as the tip speed ratio increases. In the case of the two bladed Rooftop rotor, the moment coefficient become negative around $\lambda = 0.88$, while that in the case of three bladed Rooftop rotor become negative around $\lambda = 0.96$. Also, it can be seen that the magnitude of moment coefficient increases as the numbers of blade increases. For the case of three bladed Rooftop rotors the moment coefficient increases at 30% as compared with two bladed Rooftop rotors. While that in the case of four bladed Rooftop rotor the moment coefficient increases at 35% as compared with two bladed Rooftop rotors.

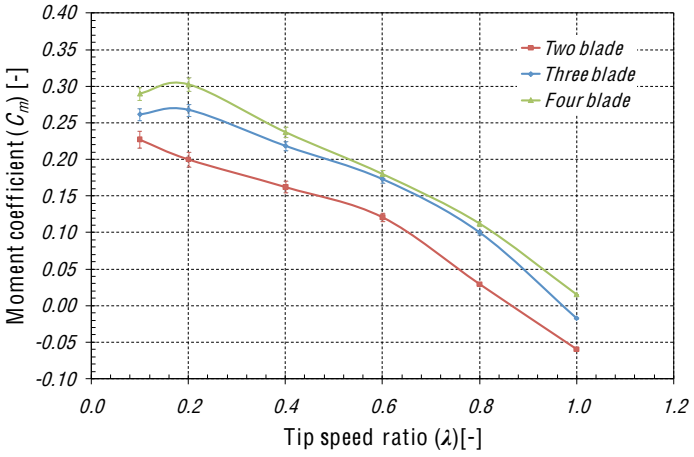

Figure 10. *Variation of moment coefficient (Cm) for two bladed, three bladed and four bladed Rooftop rotors.*

The effect to have an increase in the moment coefficient as the blade number increases, in the cases of Rooftop rotor, may be due to that a bigger amount of flow volume is captured, between blades turbine rotor.

Figure 11 shows the results obtained from Savonius rotors. According to the results, each rotor has a different behavior in specific range of tip speed ratio of wind turbine rotor in proportion of the other rotor. In the case of two bladed Savonius rotor it has a moment coefficient lower than three bladed and four bladed Savonius rotors in low tip speed ratio. While to values greater than $\lambda = 0.32$ of tip speed ratio, two bladed Savonius rotor offers a moment coefficient greater then three bladed and four bladed Savonius rotors.

On the other hand, in the case of two blade Savonius rotor, moment coefficient increases smoothly as the tip speed ratio increase up to $\lambda = 0.34$. It then starts decrease linear as the tip speed ratio continues increase, become negative around $\lambda = 0.9$. For the case of three bladed Savonius rotor, moment coefficient decrease suddenly as the tip speed ratio increases up to $\lambda = 0.21$. Then continue decreases smoothly up to $\lambda = 0.5$. Finally, decrease nearly linear as the tip speed ratio increases. Which become negative around $\lambda = 0.82$. In the case of four bladed Savonius rotor, moment coefficient decrease nearly linear as the tip speed ratio increases, become negative to $\lambda = 0.7$, approximately.

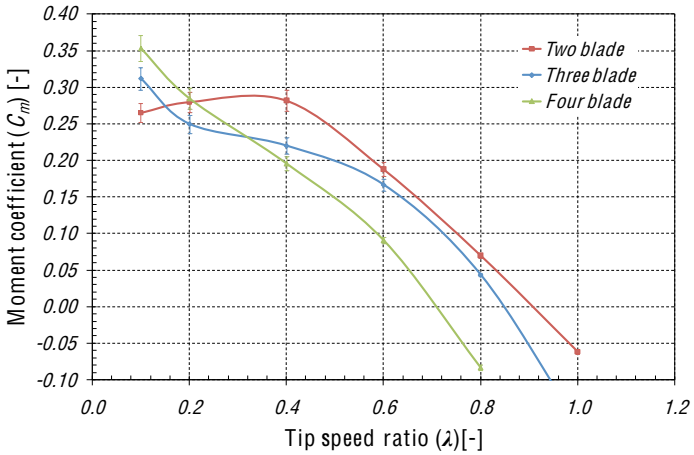

Figure 11. *Variation of moment coefficient (C_m) for two bladed, three bladed and four bladed Savonius rotors.*

Unlike to Rooftop rotor, in general, the moment coefficient obtained from Savonius rotors decreases as the blades number increases. This behavior may be due to semi-circular geometry of blade rotor, having that negative moment increases as the blades number increases, thus decreases the performance of turbine rotor.

3.4 Power coefficient as function of tip-speed ratio

Figures 12 and 13 showed the power coefficient for two bladed, three bladed and four bladed rotors as function of the dimensionless parameter tip-speed ratio. In the Figure 12 are showed the results obtained from Rooftop rotors. It can be seen, that magnitude of power coefficient decrease as the number of bladed increases. For the case of four bladed Rooftop rotors the power coefficient increases at 30% as compared with two bladed Rooftop rotors, while that in the case of three bladed Rooftop rotors the power coefficient increases at 25% as compared with two bladed Rooftop rotors. The power coefficient has its maximum value around $\lambda = 0.58$, $\lambda = 0.6$ and

$\lambda = 0.6$ for the case of two bladed, three bladed and four bladed Rooftop rotor.

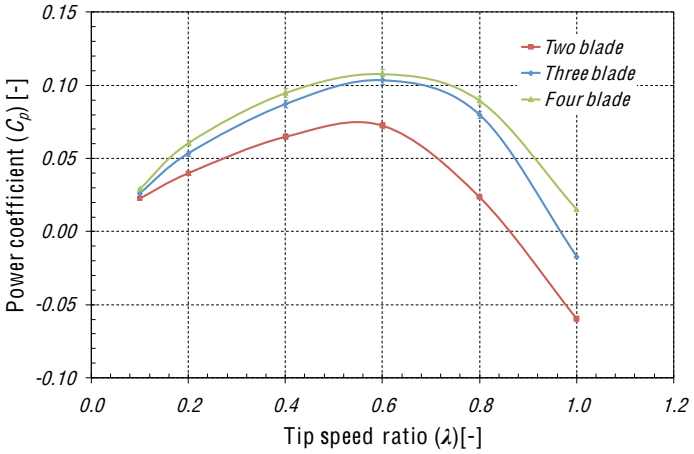

Figure 12. *Variation of power coefficient (C_P) for two bladed, three bladed and four bladed Rooftop rotors.*

Figure 13 are shows the results obtained from Savonius rotors. Unlike to Rooftop rotors, magnitude of power coefficient from Savonius rotors decreases as the number of bladed increases. For the case of four bladed Rooftop rotors the power coefficient decreases at 34% as compared with two bladed Rooftop rotor*s*, while that in the case of three bladed Rooftop rotors the power coefficient increases at 16% as compared with two bladed Rooftop rotors. The power coefficient has its maximum value around $\lambda = 0.5$, $\lambda = 0.56$ and $\lambda = 0.4$ for the case of two bladed, three bladed and four bladed Rooftop rotor, respectively.

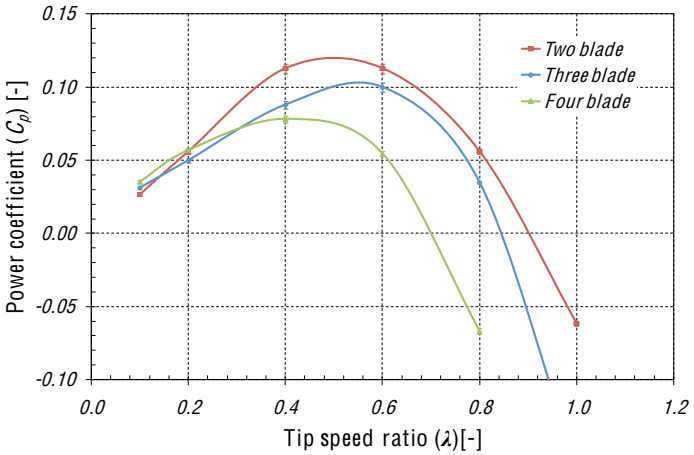

Figure 13. *Variation of power coefficient (C_P) for two bladed, three bladed and four bladed Savonius rotors.*

In general, all rotors present a similar power coefficient in the range of tip speed ratio smaller that $\lambda = 0.2$.

3.5 Comparison of power coefficient

In order to compare the results obtained from Rooftop and Savonius rotors that offer the maximum power coefficient was created the Figure 14. For this were considered the configurations with four bladed and two bladed rotors, which offers the better aerodynamic performance in the case of Rooftop and Savonius rotors, respectively.

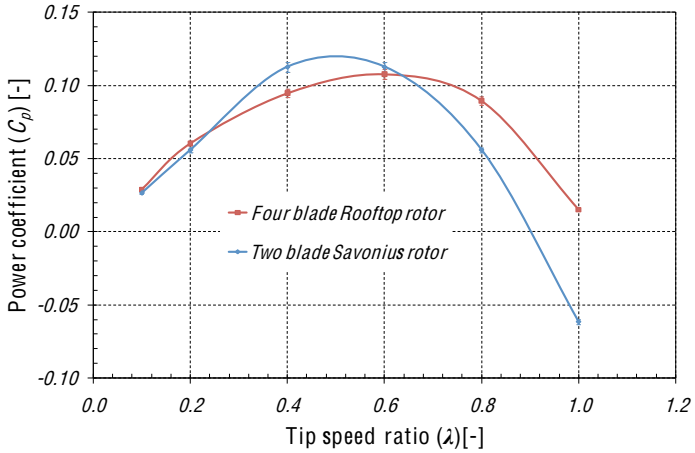

Figure 14. *Comparison of power coefficient (C_P) obtained to four bladed Rooftop and two bladed Savonius rotors.*

Comparing the results obtained, it is possible to observe that four bladed Rooftop rotor has greater power coefficient than two bladed Savonius rotor in low and high tip speed ratio (ranges from 0.1 to 0.24 and 0.64 to 1 of tip speed ratio, respectively) In a mid-range of tip speed ratio, from 0.24 to 0.64, two bladed rotor offer better performance as compared with four bladed Rooftop rotor.

4. CONCLUSIONS

In the present work, a numerical study was developed, getting the effect generated by the numbers of blade in the aerodynamic performance of Rooftop vertical axis wind turbine. The main conclusions are:

- The behavior of the flow around the Savonius rotor present a good agree to experimental results [17] on the front and back sides of the blade rotor, Figure 6, which allows having a trust major the result obtained with the computational models.
- The number of period per rotor revolution increase as the numbers of blade increases, while that amplitude of moment coefficient decrease as the numbers of blade increases. In both Rooftop and Savonius rotor.
- Rooftop and Savonius rotors have a period per rotor revolution each 180º, 120º and 90º rotor angle for the cases of two bladed, three bladed and four bladed rotors.
- The average coefficients of power and moment increase as the numbers of blade increases in the cases of Rooftop rotor. On the other hand, the average coefficient of power and moment decrease as the numbers blade increases in the cases of Savonius rotors.

- The configurations with four bladed and two bladed rotors offer the better aerodynamic performance in the cases of Rooftop and Savonius rotors, respectively.
- At low tip speed ratio, all rotors present a similar aerodynamic performance. At high tip speed ratio Rooftop rotors have greater power coefficient than Savonius rotors.

5. FUTURE WORK

In a later work, the analysis of the aerodynamic performance varying the separation gap and the overlap between rotor blade overlap between blades in the numerical models of Rooftop rotors must be developed. Also, it is going to be implement a UDF based on C language to predict the aerodynamic performance of vertical axis wind turbine that allow computed the fluid-solid coupling.

NOMENCLATURE

A	Frontal rotor area [m^2]
a	Blade gap-size [m]
b	Blade overlap [m]
$C_{1\varepsilon}$	Constant [--]
$C_{2\varepsilon}$	Constant [--]
C_p	Pressure coefficient [--]
C_P	Power coefficient [--]
c	Axial chord length of the blade [m]
D	Rotor diameter [m]
D_h	Hydraulic diameter [m]
d	Shaft diameter [m]
G_k	Turbulent kinetic energy generation
H	Height of the wind rotor [m]
M	Aerodynamic moment [N·m]
P	Power [W]
p	Length of the straight line portion [m]
p_i	Static pressure at the i^{th} tap [Pa]
p_∞	Static pressure at the infinity [Pa]
r	Rotor radius [m]
T_i	Turbulent intensity [%]
R_ε	Additional term in dissipation ration
u_i	Velocity vector [m/s]
U_∞	Free stream velocity [m/s]
x	Axial length [m]

Greek Symbols

α	Position angle for curtain a [º]
α_k	Inverse effective Prandtl number by k
α_ε	Inverse effective Prandtl number by ε
β	Position angle for curtain b [º]
γ	Angle between blade rotor [º]
δ_{ij}	Kronecker delta
ε	Dissipation rate [m^2/s^3]
η	Blade circular arc angle [º]
θ	Angular position [º]
κ	Turbulent kinetic energy [m^2/s^2]
λ	Tip speed ratio [--]
μ	Viscosity [kg/m·s]
μ_{eff}	Effective viscosity [kg/m·s]
ρ	Density [kg/m^3]
$(\tau_{ij})_{eff}$	Viscous stress tensor
ω	Angular velocity

REFERENCES

[1] J. Sargolzaei and A. Kianifar, 2009 "Modeling and simulation of wind turbine Savonius rotors using artificial neural networks for estimation of the power ratio and torque", Simulation Modelling Practice and Theory, Volume 17, Issue 7, August 2009, Pages 1290-1298.

[2] Ushiyama I. and Nagai H., 1988 "Optimum design configuration and performance of Savonius rotors", Wind Engineering, Vol. 12, Pages 59-75.

[3] Sheldahl R.E., Blackwell B.F. and Feltz L.V., 1978 "Wind tunnel performance data for two and three bucket Savonius rotors", Journal of Energy Vol. 2, Pages 160-164.

[4] Alexander A.J. and Holownia B.P., 1978, "Wind tunnel test on a Savonius rotor" Journal of Industrial Aerodynamics, Vol. 3, Pages 343-351.

[5] Modi V.J. and Fernando M.S.U.K., 1989, "On the performance of the Savonius wind turbine" ASME Journal of Solar Energy Engineering, February 1989, Vol. 111, Issue 1, Pages 71–81.

[6] Mojola O.O., 1982, "On the aerodynamic performance of the Savonius windmill rotor" Proceedings of the seventeenth Intersociety Energy Conversion Engineering Conference, Los Angeles, CA, August 8-12, 1982.

[7] Mojola O.O. and Onazanya O.E., 1984, "Performance testing of a Savonius windmill rotor in shear flow" Wind Engineering, Vol. 8, no. 2, Pages 109-121.

[8] Burcin Deda Altan and Mehmet Atilgan, 2008 "And experimental and numerical study on the improvement of the performance of Savonius wind rotor" Energy Conversion and Management, Vol. 14, Pages 3425-3432.

[9] Burcin Deda Altan and Mehmet Atilgan, 2010 "The use of curtain design to increase the performance level of a Savonius wind rotors" Renewable Energy, Vol. 35, Pages 821-829.

[10] K. Pope, V. Rodrigues, R. Doyle, A. Tsopelas, R. Gravelsins, G.F. Naterer and E. Tsang, 2010 "Effects of stator vanes on power coefficients of Zephyr vertical axis wind turbine" Renewable Energy, Vol. 35, Pages 1043-1051.

[11] V. D'Alessandre, S. Montelpare, R. Ricci and A. Secchiaroli, 2010, "Unsteady aerodynamics of a Savonius wind rotor: a new computational approach for the simulation of energy performance" Energy, Vol. 35, Pages 3349-3363.

[12] Fluent Inc Products, FLUENT® Ver. 6.3.26

[13] Fluent Inc Products, GAMBIT® Ver. 2.4.6

[14] R.A. Berdanier, K..E. Hernandez, C.P. Raye, C.P. Horvath, LM. Graham, TP. Hatlee, N.H. Phan, P. M. Pelken and T.Q. Dang, 2010, "Integrating vertical-axis wind turbines and photovoltaic solar cells to power a self-sustaining outdoor light source" Presented at the 7th International Conference on Indoor Air Quality, Ventilation and Energy Conservation in Buildings, August 15-18, 2010 (In press).

[15] Aron Zingman, 2007, "Optimization of a Savonius rotor vertical-axis wind turbinefor use in water pumping systems in rural Honduras" Bachelor of Science.

[16] D. Choudhury, 1993, "Introduction to the renormalization group method and turbulence modeling" Fluent Inc. Technical Memorandum TM-107.

[17] Fernando M.S.U.K, 1987, "On the performance and wake aerodynamics of the Savonius wind turbine" Doctoral Thesis.